Stem Cell Reports
Article

ISSCR

OPEN ACCESS

Keratin-14-Positive Precursor Cells Spawn a Population of Migratory Corneal Epithelia that Maintain Tissue Mass throughout Life

Alexander Richardson,[1] Erwin P. Lobo,[2] Naomi C. Delic,[3,4] Mary R. Myerscough,[2] J. Guy Lyons,[3,4,5] Denis Wakefield,[1] and Nick Di Girolamo[1,*]

[1]School of Medical Science, University of New South Wales, Sydney, NSW 2052, Australia
[2]School of Mathematics and Statistics, University of Sydney, Sydney, NSW 2050, Australia
[3]Immune Imaging Program, Centenary Institute, Sydney, NSW 2050, Australia
[4]Department of Dermatology, Sydney Medical School, University of Sydney, Sydney, NSW 2050, Australia
[5]Cancer Services, Royal Prince Alfred Hospital, Sydney, NSW 2050, Australia
*Correspondence: n.digirolamo@unsw.edu.au
http://dx.doi.org/10.1016/j.stemcr.2017.08.015

SUMMARY

The dynamics of epithelial stem cells (SCs) that contribute to the formation and maintenance of the cornea are poorly understood. Here, we used K14CreER^{T2}-Confetti (Confetti) mice, sophisticated imaging, and computational modeling to trace the origins and fate of these cells during embryogenesis and adult life. We show that keratin-14 (K14$^+$)-expressing progenitors are defined and widely distributed across the E16.5 cornea, after which they undergo cycles of proliferation and dispersal prior to eyelid opening. K14$^+$ clonal patches disappear from the central cornea and are replaced by limbal-derived K14$^+$ streaks, a finding that aligned with bromodeoxyuridine label-retaining studies. We also elucidated the mechanism by which SC clones are lost during life and propose this is due to population asymmetry and neutral drift. Finally, we established that the occurrence of an equatorial migratory mid-line is a consequence of apoptosis in a narrow nasal-temporal region, the site where eyelids meet during blinking.

INTRODUCTION

Visualizing the generation and maintenance of the corneal epithelium in a living organism, especially in real time, is a challenging endeavor. The cornea forms during the last major inductive event that constitutes eye genesis, i.e., when cells of the lens vesicle detach from the overlying surface ectoderm, leaving a void that is occupied by invading mesenchymal-derived neural crest cells (Lwigale, 2015; Zieske, 2004). In mammals, the presumptive corneal epithelium forms from surface ectoderm and comprises a dual layer of elongated, undifferentiated cells that are protected by the enveloping eyelids (Zieske, 2004). Following eyelid opening, the corneal epithelium is exposed to exogenous stimuli including O_2, particulate matter and microbes, and endogenous mechanical forces due to blinking, thereby triggering cellular expansion from two to six layers. This coincides with changes in cell shape, whereby basal cells become columnar, while supra-basal and superficial cells acquire a flattened wing and squamous morphology, respectively (Zieske, 2004).

When the mammalian cornea reaches maturity and its epithelial SC repository is confined to the limbus, precursor cells divide and their descendants differentiate into transit-amplifying cells (TACs), which migrate centripetally toward the apex of the cornea. During their journey, TACs divide and give rise to supra-basal terminally differentiated cells that are then sloughed from the ocular surface (Auran et al., 1995; Beebe and Masters, 1996; Bron, 1973; Buck, 1985; Mann, 1944; Thoft and Friend, 1983). Centripetal migration is likely driven by the location of SCs in the limbal margin, so-called limbal epithelial SCs (LESCs), and the limited replicative ability of TACs, which together create a population pressure gradient that is directed toward the central cornea (Lobo et al., 2016).

One significant shortcoming of previous research is that some data were collected from either direct visual observations or by standard light microscopy after enucleation (Buck, 1985; Mann, 1944). Using approaches in which non-specific (X-linked or ubiquitous) genetic reporters randomly labeled cell lineages, researchers observed that clones transcended the cornea in a curvilinear fashion (Collinson et al., 2002; Mort et al., 2009; Nagasaki and Zhao, 2003). It was also noted that the pattern formed was not static; rather clones disappeared while others become broader (Collinson et al., 2002; Mort et al., 2009). However, because the precise cell type from which these clones originated was not defined, it was speculated that variation in the striping pattern was due to either SCs or early TACs undergoing cycles of proliferation, quiescence, and cell death (Dora et al., 2015; Mort et al., 2009), rendering interpretations of these results difficult.

Despite there being no unifying LESC-specific antigen, keratin-14 (K14) is considered a reliable discriminatory marker for these cells in humans (Eghtedari et al., 2016) and mice (Kurpakus et al., 1994; Tanifuji-Terai et al., 2006). Here, we employed the K14 promoter-driven CreER^{T2} construct (Indra et al., 2005) to drive expression of the multi-color Confetti transgene (Snippert et al., 2010) in K14$^+$ epithelial precursor cells as a method to trace

their fate in the mouse cornea. Previously, this model was used to define the origins and migration of $K14^+$ SCs and their descendants (Di Girolamo et al., 2015), and the imposed forces that propel these cells toward the central cornea (Lobo et al., 2016) during a narrow 6–20 week time frame. The current investigation mapped the spatio-temporal distribution of genetically marked $K14^+$ cells and their progeny from embryonic day (E16.5) to approximately 70 weeks of age. We established the origins, distribution, proliferation, and dissemination activity of progenitor-derived clones during development and their limbal sequestration at the approximate time of eyelid opening. In addition, several other dynamic age-related changes were recorded; firstly, the loss of SC clones, the mechanism of which aligns with the neutral drift theory, and secondly, the formation of an equatorial mid-line, caused by low-level apoptosis in this narrow region. Taken together, our results provide visual and mechanistic insights into previously unexplained developmental and homeostatic phenomena that transpire in the mammalian cornea.

RESULTS

Distribution of $K14^+$ Epithelial Precursor Cells during Corneal Development

To determine when and from where $K14^+$ embryonic epithelial cells originate in the developing cornea, time-mated female Confetti mice were administered tamoxifen (TAM) at E15.5 to induce expression of the reporter genes in developing embryos. At E16.5, fluorescent $K14^+$ progenitor cells and their descendants were observed across the presumptive corneal epithelium, forming small isolated clones comprising 4.6 ± 0.7 cells (Figures 1A and 1H), which proliferated to 16.4 ± 2.6 cells by E18.5 ($p < 0.0001$) (Figures 1B and 1H). During this period, the total number of fluorescent epithelial cells significantly increased from 173 ± 21.5 at E16.5 to 336 ± 69.1 at E18.5 ($p = 0.0012$) (Figure 1G), indicating clonal proliferation. At E19.5, few cohesive multi-cellular clones (1.3 ± 0.1 cells) remained ($p = 0.027$); instead, labeling was predominantly confined to individual cells that were scattered across the ocular surface (Figures 1C and 1H). The number of fluorescent cells at E19.5 remained constant when compared with E18.5 (351 ± 63.8 versus 336 ± 69.1, respectively) ($p = 0.68$) (Figure 1G), indicating that clonal dispersion was likely achieved by random cell movement, rather than proliferation. At post-natal day (P)7, small clonal patches of 6.0 ± 0.97 fluorescent cells (Figures 1D and 1H) formed and expanded into larger colonies which contained 28.4 ± 3.2 cells at P14 ($p < 0.0001$) (Figures 1E and 1H). During this period, fluorescent clones were seen across the corneal surface; instead of a random orientation, clonal aggregates began to align radially toward the apex of the cornea (Figures 1E and 1F). In transverse tissue sections, rare fluorescent basal cells were identified in the tri-layered corneal epithelium, however, most fluorescence arose from superficial cells of the developing post-natal cornea (Figure 1I).

Centrally Located $K14^+$ Embryonic Clones Are Replaced by Limbal-Derived Equivalents during Early Post-natal Life

In our previous study, we identified rare $K14^+$ patches within the central cornea of adult mice (Di Girolamo et al., 2015), suggesting that a limited number of progenitors are located away from the limbus. Following our observation that the developing corneal epithelium contains widely dispersed $K14^+$ fluorescent clones (Figure 1), Confetti pups at P7 were administered TAM and their corneas monitored by intra-vital microscopy for 10 weeks (Figure 2). At 1 week post TAM, fluorescent clones were detected across the cornea (Figure 2A), similar to those in P14 pups following *in utero* transgene induction (Figure 1E). However, at 5 weeks post TAM, the central fluorescence intensity was significantly diminished ($p < 0.0001$) (Figure 2D), indicating a loss of central $K14^+$ clones, and fluorescent streaks emerged from the peripheral cornea (Figure 2B). This aligns with basal limbal cell proliferation, which is significantly increased at 6 weeks of age compared with both 3 week ($p < 0.01$) and older mice ($p < 0.05$) (Figure S1). Limbal-derived fluorescent clones migrated centripetally and reached the central cornea within 10 weeks (Figure 2C). During this time, most centrally located fluorescent clones disappeared, however $K14^+$ cell density significantly increased 10 weeks post TAM ($p = 0.046$) due to the influx of limbal-derived clones (Figure 2D). Moreover, the corneal epithelium expanded from two to three layers in 2-week-old mice in which superficial cells fluoresced (Figure 2E) to a multi-layered tissue in 11-week-old animals with fluorescence-bearing cells in each layer (Figure 2F). The superficial nature of fluorescent $K14^+$-derived cells aligns with our previous findings in the developing human cornea (Eghtedari et al., 2016). Furthermore, these data conclusively illustrate the loss of centrally located $K14^+$ corneal epithelial SCs (CESCs) during early post-natal life and their replacement by LESCs from the main peripheral repository (Collinson et al., 2002; Mort et al., 2009).

$K14^+$ Cells Segregate to the Limbus during Aging

We investigated the localization of $K14^+$ precursor cells during aging to ascertain when they consolidated to the limbus (Figure 3) and found that in 2-week-old transgenic mice, $K14^+$ cells were evenly distributed throughout the cornea (Figures 3A and 3B). In 10-week-old mice, a bimodal distribution of $K14^+$ cells was noted (Figures 3C and 3D),

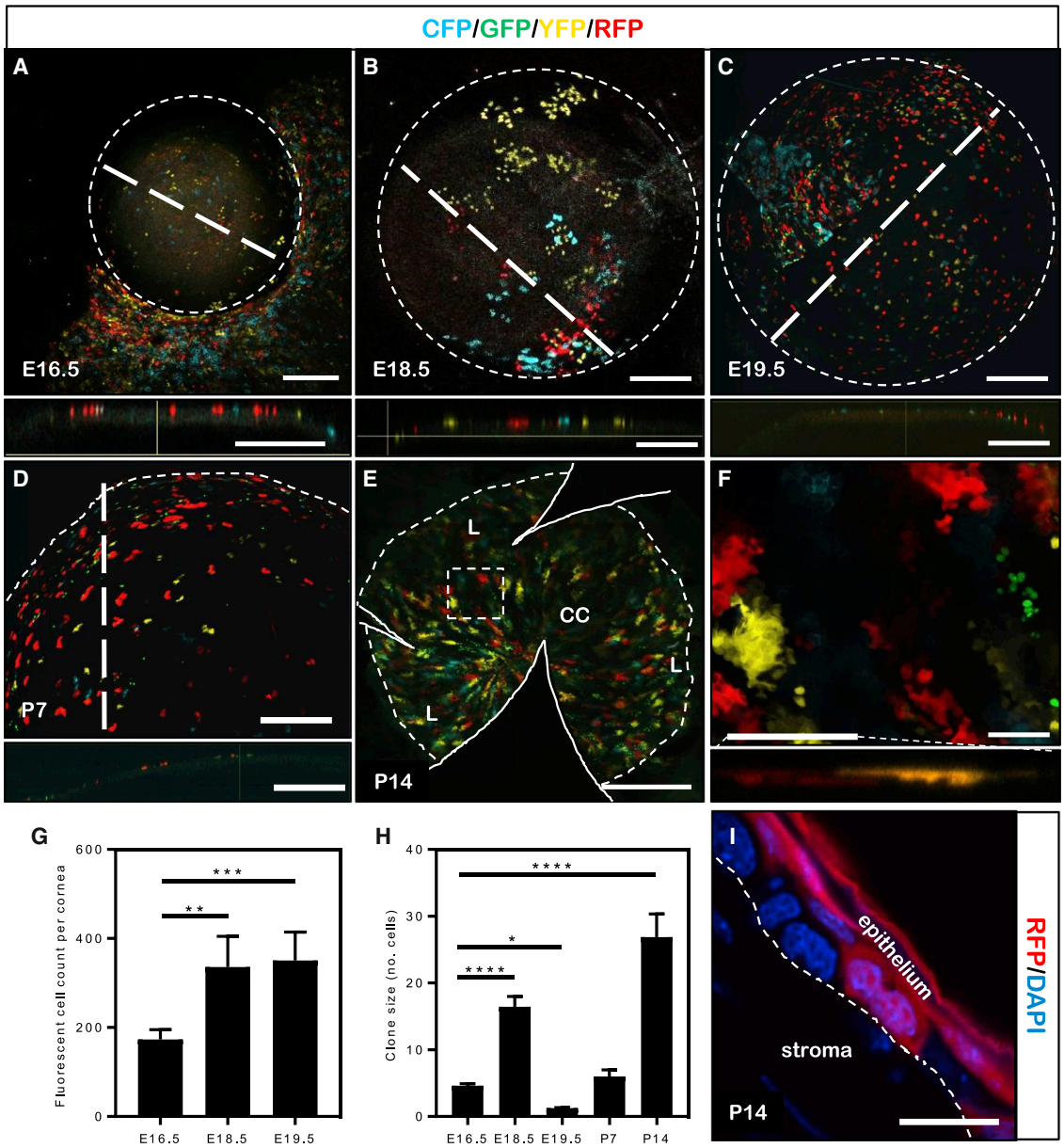

Figure 1. Spatiotemporal Distribution of K14$^+$ Precursor Cells during Embryonic and Neonatal Development

(A–C) Confetti embryos (n=4 eyes/time point) harvested at E16.5 (A), E18.5 (B), and E19.5 (C) with corneas imaged by confocal microscopy. Optical cross-sections (A–C, lower panels) were acquired at the plane marked by thick hatched lines. Thin circular hatched line represents the cornea boundary.

(D–F) Neonatal corneas (n = 4 eyes/time point) imaged at P7 (D) and P14 (E and F). An optical cross-section (D, lower panel) was obtained along the plane marked by the thick hatched line. Whole corneas from P14 mice were flat-mounted (E and F). Solid white lines (E) depict incisions made to facilitate flat-mounting. The hatched box (E) is magnified in (F). Optical cross-section (F, lower panel) was obtained at the plane marked by the solid white line.

(G) Total number of fluorescent cells within developing mouse corneas (n = 4 corneas/time point, ± SD, $^{**}p < 0.01$ and $^{***}p < 0.001$, one-way ANOVA with Holm-Sidak multiple comparison test).

(H) Clonal size represented by the number of cells (n = 10 clones/cornea, ± SD, $^{*}p < 0.05$ and $^{****}p < 0.0001$, one-way ANOVA with Holm-Sidak multiple comparison test).

(I) Representative cryo-section prepared from P14 mouse eye; only RFP (red) is displayed, and tissue was counterstained with DAPI (blue) to highlight cell nuclei. The white hatched line represents the epithelial basement membrane.

Scale bars: (A–D) 300 μm, (E) 400 μm, (F) 30 μm, (I) 10 μm.

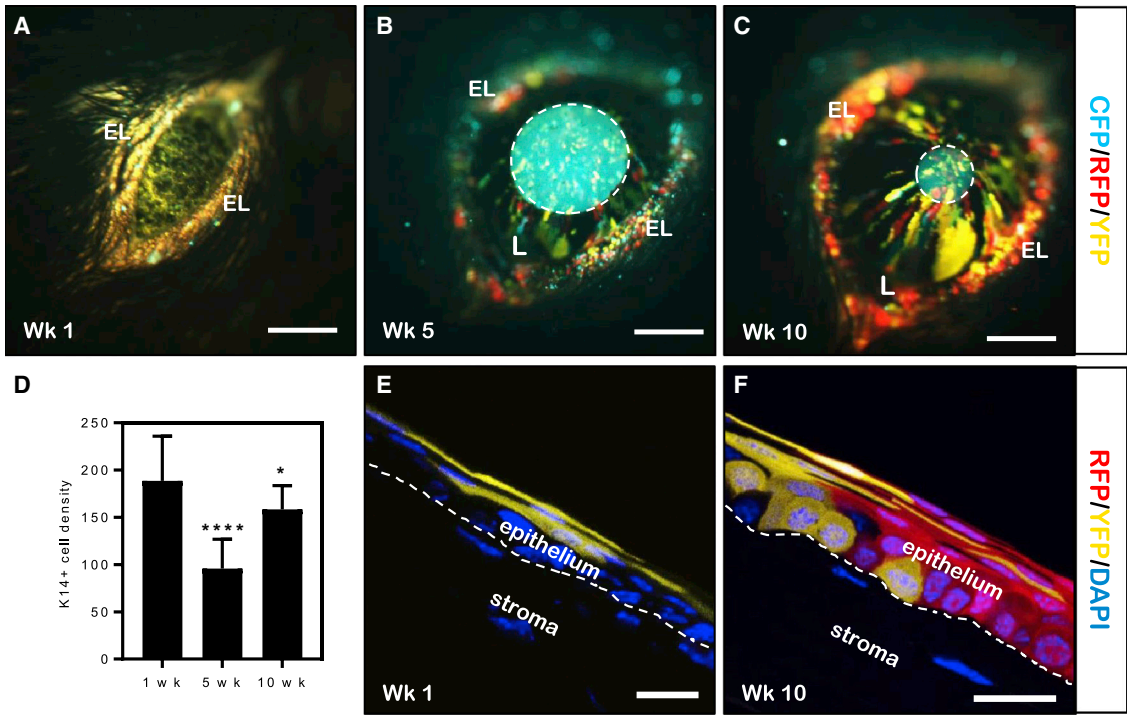

Figure 2. Predominance of Limbal-Derived Fluorescent Clones during Early Post-natal Development

(A–C) Confetti mice (n = 3 corneas/time point) were administered TAM at P7 and monitored by intra-vital microscopy at 1, 5, and 10 weeks. Hatched circle in (B) and (C) outlines the intra-ocular lens, which auto-fluoresces. EL, eyelid; L, limbus.

(D) Mean fluorescence intensity within a 1 mm central region of cornea (n = 3 corneas/time point, ± SD, *p < 0.05, ****p < 0.0001, one-way ANOVA with Holm-Sidak multiple comparison test).

(E and F) Cryo-sections of whole eyes (n = 3 corneas/time point) at week 1 (E) and week 10 (F) post TAM counterstained with DAPI. The white hatched line represents the epithelial basement membrane.

Scale bars: (A–C) 400 μm, (E and F) 15 μm. See also Figure S1.

indicating the progressive loss of these cells from the mid-periphery; an observation that aligns with our previous results in 8-week-old Confetti mice (Lobo et al., 2016). By 20 weeks, fluorescent cells were rarely observed in the central cornea and primarily occupied the limbal region (Figures 3E and 3F, zone 8), a pattern that remained constant in 60-week-old mice (Figures 3G and 3H). In bromodeoxyuridine (BrdU) pulse-chase experiments, most label-retaining cells (LRCs) were confined to the limbus, irrespective of age (Figure S2). However some LRCs occupied the central cornea, similar to a recent report (Li et al., 2017).

Age-Related Stem Cell Dynamics in the Murine Cornea

We previously demonstrated that during a narrow time frame of 6–20 weeks, the corneal epithelium is maintained by a population of $K14^+$ limbal progenitor cells (Di Girolamo et al., 2015; Lobo et al., 2016). To investigate how these cells behave long term, 6-week-old Confetti mice were administered TAM, and their corneas were monitored monthly over 60 weeks by intra-vital microscopy. Fluorescent cells emerged from the limbal margin and migrated toward the central cornea along narrow linear paths (Figures 4A and 4B) at a rate of 12.6 ± 1.3 μm/day. This velocity was maintained throughout the initial 20-week monitoring period (r^2 = 0.98) (Figure S3D) and clones reached the apex 16–20 weeks post TAM (Figure 4C). Furthermore, the central cornea contained small fluorescent colonies until approximately 12–16 weeks post TAM (Figures 4A and 4B). Interestingly, age-related changes to clonal activity were also noted (Figures 4D–4F). At 16 weeks post TAM, corneas contained 66.5 ± 4.9 fluorescent streaks, which significantly decreased in number to 35.9 ± 12.9 at 60 weeks post TAM ($p < 0.0001$) (Figure 4G). This observation was concomitant with fluorescent clones increasing in width from 115 ± 28.5 μm at 16 weeks post TAM to 307 ± 36.4 μm ($p < 0.0001$) at 60 weeks post TAM (Figure 4H).

A second group of mice was injected with TAM then killed at various time points between 1 and 60 weeks post TAM, and their eyes were enucleated and scanned by light-sheet microscopy. Initially, fluorescent cells were located across the epithelium (Figure 5A), which first formed patches (Figure 5B) and by 5 weeks developed

into streaks (Figure 5C) that migrated centripetally (Figure 5D), reaching the central cornea by 20 weeks post TAM (Figure 5E). Corneas imaged by this method contained 78.3 ± 2.51 fluorescent clones at 10 weeks post TAM, which decreased to 31 ± 11 ($p < 0.0001$) at 60 weeks post TAM (Figures 5D–5I). This coincided with increased streak width, from 113 ± 13.2 μm at 10 weeks post TAM to 303 ± 17.6 μm ($p < 0.0001$) at 60 weeks post TAM (Figures 5D–5I). Clone width at the limbus increased linearly with the square root of time (Figure 5K), aligning with the notion of neutral evolutionary drift that occurs in self-renewing tissues through population asymmetry, during which SC-derived clones can only expand or contract in one dimension (Klein and Simons, 2011), in this case circumferentially throughout the limbal SC niche.

Our mice displayed several other fascinating clonal patterns. These included a centrally located vortex, prominent in corneas of older mice (Figures 4D–4F, 5F, S3A, and S3B), that generally occurred bilaterally with a random direction of rotation (Figure S3E). Furthermore, some fluorescent streaks were detached from the periphery (Figure S3A, arrows), indicating that their $K14^+$ precursors were being depleted or were undergoing cycles of quiescence during aging. Alternatively, symmetric SC division giving rise to two TACs (both of which depart the limbus) may explain the disappearance of a clone and its replacement with a different colored neighbor (Figure S3C).

The Corneal Epithelial Mid-line Is Formed by Apoptosis

The third peculiarity was the deviation of fluorescent streaks from their typically radial linear path, i.e., the tendency to bend toward the nasal-temporal (N-T) axis to form an equatorial demarcation line. Again, this was especially common (and most obvious) in aged mice with a complete streaking pattern (Figure 6A). This mid-line is remarkably similar to the Hudson-Stähli line (Every et al., 2005; Gass, 1964) that appears in the lower two-thirds of the human cornea (Rose and Lavin, 1987b). It is thought to manifest as a consequence of cellular stress due to blinking and is likely to be induced by apoptosis (Ren and Wilson, 1996) and/or increased desquamation (Yamamoto et al., 2002), producing an area of attrition thereby provoking epithelial cells to preferentially migrate toward this region. To address this posit, mice at 8, 20, and 50 weeks of age were euthanized and their eyes marked with a needle punch along the N-T axis prior to enucleation, fixation, and terminal deoxynucleotidyl transferase dUTP nick end-label (TUNEL) staining (Figures 6B and 6C). Representative images were taken along the N-T and superior-inferior (S-I) axes (Figure S4A) to determine the distribution and number of apoptotic cells. $TUNEL^+$ epithelia represented a small proportion of the total number of cells and were only observed in the superficial corneal epithelium (Figure 6C). $TUNEL^+$ cells were increased along the N-T axis compared with the S-I axis in 8-week-old mice, however this did not reach statistical significance (Figure 6D). A significantly higher percentage of $TUNEL^+$ cells were detected along the N-T axis in 20- and 50-week-old mice compared with the S-I orientation (Figures 6E and 6F). Furthermore, 20- and 50-week-old mice had a higher total number of apoptotic cells compared with 8-week-old mice, although this did not reach statistical significance (Figure S4B).

To establish what effect a higher proportion of apoptotic cells would have on migratory activity along the N-T axis, we applied our validated mathematical model (Lobo et al., 2016) to conduct simulations (Figures 6G–6P). Control simulations with 1,000 time steps (Figure 6J, Movie S1) were divided into four equidistant concentric zones (from peripheral to central) and eight radial sectors (two vertical, two horizontal, and four diagonal) (Figure 6G). For every corneal epithelial cell in each of the eight zones, we determined which sector housed the LESCs from which it was derived. In control corneas, there was a tendency for cells in a sector to be derived from LESCs located in the same sector, and any drift of the progeny of a LESC to another type of sector was compensated for by a reciprocal drift of cells back. This was the case in all zones from the periphery to the center (Figure 6H). We further scrutinized the central zone for the average percentage of cells derived from progenitors from within the N-T and S-I axes, finding no significant difference irrespective of the region or direction assessed (Figure 6I). Next, simulations were modified to incorporate 0.1% loss of cells per time step along the horizontal (N-T) axis (Movie S2). The central zone had a significantly higher rate of cell flux along the vertical than the diagonal or horizontal axes (Figure 6K, blue bars), indicating that more cells were derived from the vertical sectors than the diagonal or horizontal sectors. The remaining concentric zones also displayed significantly higher relative rates of cell loss or gain along both the vertical and diagonal axes compared with the horizontal orientation (Figure 6K, green, red, and purple bars). Furthermore, there were significantly fewer cells ($p < 0.0001$) in the central region derived from progenitors along the N-T axis compared with the S-I axis (Figure 6L). These computational analyses demonstrate significantly higher cell turnover along the horizontal axis, resulting in the formation of a mid-line over time (Figures 6M–6P, Movie S2), which is remarkably similar to the pattern that evolves on corneas of our transgenic mice.

DISCUSSION

Herein, we examined the developmental and age-related dynamics of corneal epithelial progenitor cells using the

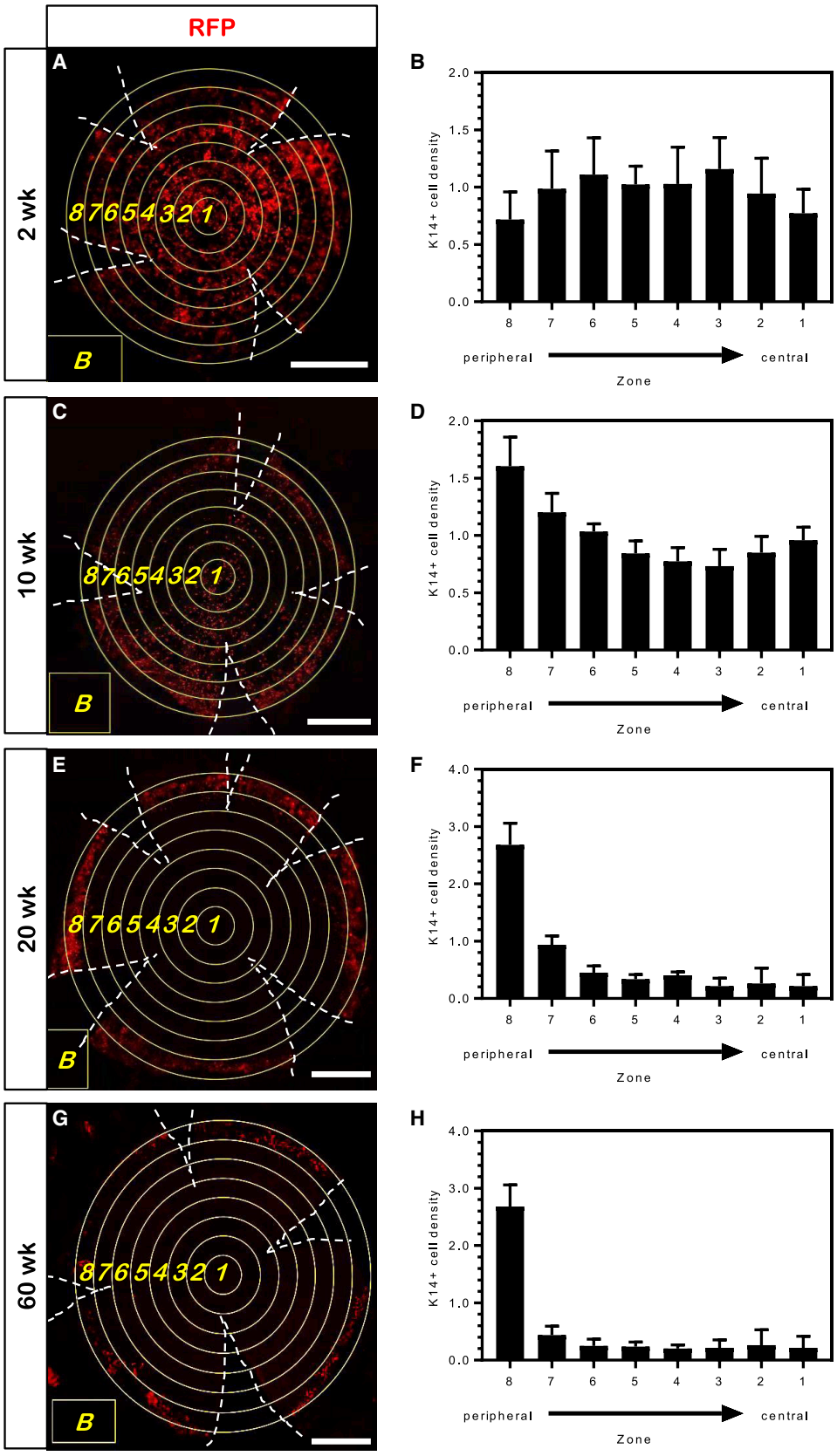

(legend on next page)

Confetti mouse, a model that delivers stable, long-term labeling of K14$^+$ basal epithelial cells and their progeny. While K14 seems to be a reliable marker of basal limbal epithelia in a number of species (Eghtedari et al., 2016; Hsueh et al., 2004; Tanifuji-Terai et al., 2006), we acknowledge that it may not be SC specific, since early generation TACs are also likely to express high levels of this antigen. However, given the longevity of genetically marked migratory clones, our data support the notion that we are labeling a population of progenitor cells. Using this model, together with *in silico* simulations (Lobo et al., 2016), we followed the destiny of these cells in real time and established the mechanism for both age-related clonal expansion and the formation of a central mid-line, thereby providing new insights into the basic biology of the mammalian corneal epithelium.

Our laboratory previously observed an interesting spatiotemporal pattern of K14 expression in the developing human corneal epithelium, being superficial and widespread at the earliest time point of examination (8 weeks' gestation) before transitioning to the basal limbal epithelial cells in fetal (24 weeks' gestation), neonatal, and adult specimens (Eghtedari et al., 2016). Using our transgenic mouse model, we noted a similar differential profile of K14$^+$ progenitor-derived fluorescent clones in embryonic, neonatal, and aged mice (Figures 1, 2, and 3). In conjunction with these observations, we demonstrated that K14-associated clonal patches expanded and fragmented in a biphasic manner (Figure 1H). The similar number of fluorescent cells within the cornea before and after clonal fragmentation indicates that this phenomenon likely occurs through random cellular movement rather than proliferation (Figure 1G). In agreement with our findings, others used the *Ubi:Zebrabow-M;ubi:CreER* zebrafish reporter line and demonstrated dispersal of cohesive clones and their subsequent replacement by limbal-derived radial stripes (Pan et al., 2013). This suggests that even though corneal epithelial development proceeds in a temporally restricted manner, the general mechanism is conserved across vertebrates.

Our investigations also verified the concept that the corneal epithelium is immature at birth and develops progressively during post-natal life (Collinson et al., 2002; Eghtedari et al., 2016; Tanifuji-Terai et al., 2006). Upon inducing the Confetti fluorescent reporter proteins in 1-week-old mice, K14$^+$ progenitor-derived clonal patches were readily visible and widely distributed across the cornea immediately following eyelid opening (Figure 2A). Five weeks later, limbal-derived clones developed into migratory streaks that possessed directionality, even though their centrally located counterparts (still visible as patches) persevered until approximately 10 weeks post TAM (Figures 2B and 2C). The emergence of limbal-derived clones, together with the loss of those located in the central cornea, coincided with increased cell proliferation at the limbal margin, especially in 6-week-old mice (Figure S1). Furthermore, BrdU pulse-chase experiments demonstrated that LRCs were predominantly confined to the limbus regardless of age (Figure S2). Notably, some LRCs were detected in the central cornea and persisted even in older mice, a result corroborated by others (Li et al., 2017). However, a longer chase period may have diluted the label to a point where these cells are no longer detectable.

These longitudinal lineage-tracing studies support and build upon previous investigations using *LacZ* mosaic reporter mice, whereby small patches of *LacZ*$^+$ cells persevered within the central cornea until approximately 10 weeks of age (Collinson et al., 2002). The use of our SC-specific mouse model unequivocally demonstrates that progenitor cells reside in the central cornea during early post-natal life, lending qualified support to previous evidence that controversially concluded the mammalian cornea is maintained by centrally located SCs rather than by LESCs (Majo et al., 2008). Notably, Majo's experiments involved grafting a limbal or central corneal biopsy from β-gal-*Rosa26* mice into athymic recipient mice. The authors reported emigration of β-gal$^+$ cells from the limbal graft but only when the cornea was challenged and not during steady state, implying that LESCs are not required for maintaining the normal corneal epithelium. When central corneal buttons from β-gal$^+$ mice were grafted into a recipient cornea, cells emerged from the graft. However, given that the authors used 16-week-old mice, it is possible that a limited number of progenitor cells remained within the central cornea (Majo et al., 2008).

Figure 3. K14$^+$ Progenitor Cell Distribution in the Corneal Epithelium of Confetti Mice during Aging

(A, C, E, and G) Whole flat-mount corneas from Confetti mice from 2-, 10-, 20-, and 60-week-old mice 1 week post TAM (n = 3/time point); only the RFP channel is displayed. Hatched white lines indicate incisions made to the cornea to facilitate flattening. Equidistant, concentric (yellow) circles were superimposed over the cornea from the limbal margin to the center using FiJi software. The yellow box marker "*B*" was the area used to establish background fluorescence. Concentric circles (1–8) spanning the limbus to central cornea correspond to the zones indicated on the x axis of each histogram in (B, D, F, and H). Scale bars, 500 μm.

(B, D, F, and H) K14$^+$ cell density of each of the four channels acquired within each concentric region (n = 4 channels, ± SD). See also Figure S2.

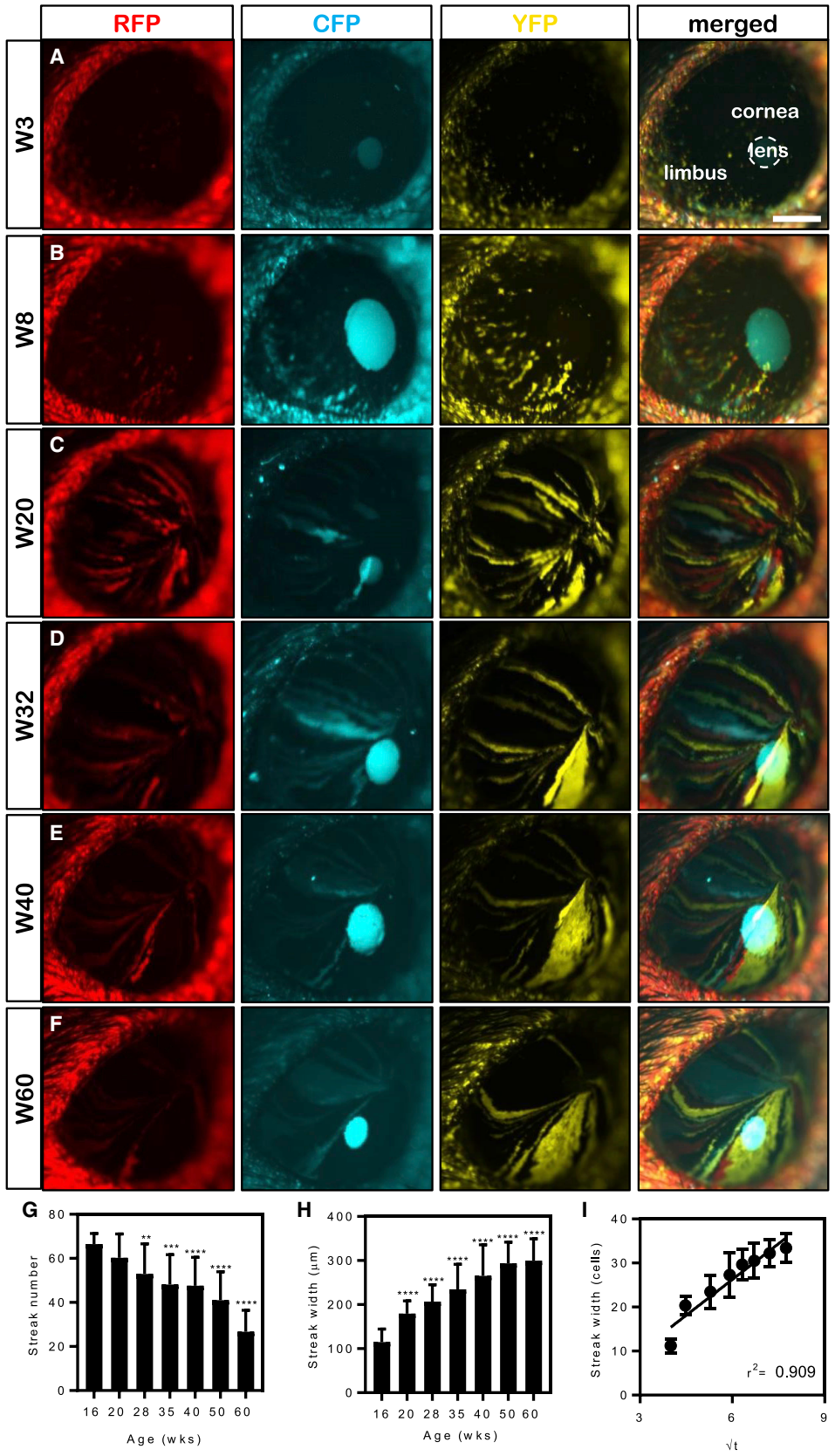

(legend on next page)

Initial attempts to fate-map corneal epithelial progenitors used either X-linked (Collinson et al., 2002; Mort et al., 2009) or ubiquitously expressed (Nagasaki and Zhao, 2003) single color reporter models, and while these studies provided basic insights into clonal behavior, their non-specific nature should be taken into consideration when extrapolating the results. This limitation has been addressed with our Confetti mouse model, which allows the real-time visualization of SC dynamics throughout a mouse's life (Figure 4). Using intra-vital microscopy, we demonstrated the formation of fluorescent radial stripes that emerged from the limbus and migrated toward the central cornea (Figures 4 and 5), identical to and traveling at a similar speed to those detected in our previous study (Di Girolamo et al., 2015). However, due to the extended monitoring, a decline in fluorescent streak number with a concomitant increase in width was observed (Figures 4 and 5), a phenomena that has previously been attributed to SC quiescence or SC loss over time (Collinson et al., 2002; Mort et al., 2009). If indeed this is the explanation, any remaining SCs would need to augment their proliferative activity to maintain tissue mass. We propose an alternative mechanism whereby depleted SCs are replaced to ensure constant and life-long regenerative activity. Our results (Figures 4I, 5K, and S2) revealed that LESC dynamics are consistent with population asymmetry and evolutionary neutral drift (Klein and Simons, 2011). Neutral drift is a phenomenon by which the number of clones in a tissue diminishes in a predictable fashion over time, as lost SCs are replaced by their neighbors undergoing symmetrical division to produce two progenitor cells (Doupe et al., 2012). When tissues are labeled with a multi-color reporter, this phenomenon is visualized as an increase in clone size together with a decrease in the number of clones over time. Furthermore, if this is the case, the cornea is more comparable with simple glandular epithelia such as the intestinal crypts (Snippert et al., 2010), rather than other stratified epithelia such as the inter-follicular epidermis. This is due to the one-dimensional arrangement of SCs as a circumferential band around the cornea (Klein and Simons, 2011). Low-level symmetric SC division is a viable mechanism in the cornea, which was modeled in our Confetti mouse (Lobo et al., 2016).

Another striking observation was the occurrence of a whorl that formed near the apex of most adult murine corneas (Figure S3). This has been noted in a number of transgenic mouse (Collinson et al., 2002; Mort et al., 2009; Nagasaki and Zhao, 2003) and rat (Iannaccone et al., 2012) models, and in human disease (Dua and Gomes, 2000), however to date a solid explanation has not been offered. Intriguingly, sub-basal corneal nerves generate a nearly identical radial pattern commonly forming a central swirl of axons (Patel and McGhee, 2005), and basal corneal epithelia can act as surrogate Schwann cells for sub-basal corneal nerves (Stepp et al., 2016); therefore it is tempting to speculate that interactions between basal corneal epithelial cells and adjacent neurons are responsible for establishing these vortices. However, we recently demonstrated that only three conditions are necessary to induce a radial streaking pattern: (1) peripherally located progenitor cells, (2) TACs with a limited number of divisions, and (3) a cell population gradient that is lower in the central cornea (Lobo et al., 2016). Our mathematical model provided no indication that other guidance cues are necessary to instigate cell movement, at least under physiological conditions.

The other curious formation, for which an explanation has never been offered, was that of a horizontal demarcation line along the N-T axis, toward which fluorescent streaks converged (Figure 6A), similar to that which evolved in aged *LacZ* reporter mice (Collinson et al., 2002; Mort et al., 2009). In providing an explanation for this phenomena, we observed similarities to the Hudson-Stähli line that develops in human corneas, i.e., the approximate region on the ocular surface where eyelids meet during blinking (Gass, 1964). Certainly, Davanger and Evensen (1971) observed emigrating melanin-containing epithelia from the inferior limbal arc of a dark-skinned individual, and their horizontal bending and merging at the Hudson-Stähli line. The Hudson-Stähli line in humans is visible due to the accumulation of cytoplasmic iron in basal cells and is thought to arise from cell stress, e.g.,

Figure 4. Real-Time Clonal Evolution in Confetti Mouse Corneas

(A–F) Intra-vital microscopy of Confetti mice following a chase period of 3 (A), 8 (B), 20 (C), 32 (D), 40 (E) and 60 (F) weeks. Expression of RFP (first column), CFP (second column), YFP (third column), and merged images (last column) are displayed. Hatched circle represents the outline of the intra-ocular lens. RFP, red fluorescent protein; CFP, cerulean fluorescent protein; YFP, yellow fluorescent protein.

(G) Fluorescent streak number (n = 6 corneas/time point, ± SD, $^{**}p < 0.01$, $^{***}p < 0.001$, and $^{****}p < 0.0001$, one-way ANOVA with Holm-Sidak multiple comparison test).

(H) Fluorescent streak width (n = 6 corneas/time point, ± SD, $^{****}p < 0.0001$, one-way ANOVA with Holm-Sidak multiple comparison test).

(I) The width of the fluorescent streaks (in number of cells) against the inverse square root of the appropriate time point. Streak width was transformed from micrometers to number of cells based on the average width of a corneal epithelial basal cell of 10 μm. Data points represent the mean (n = 3 corneas/time point, ± SD, linear regression).

Scale bars: (A–F) 400 μm. See also Figure S3.

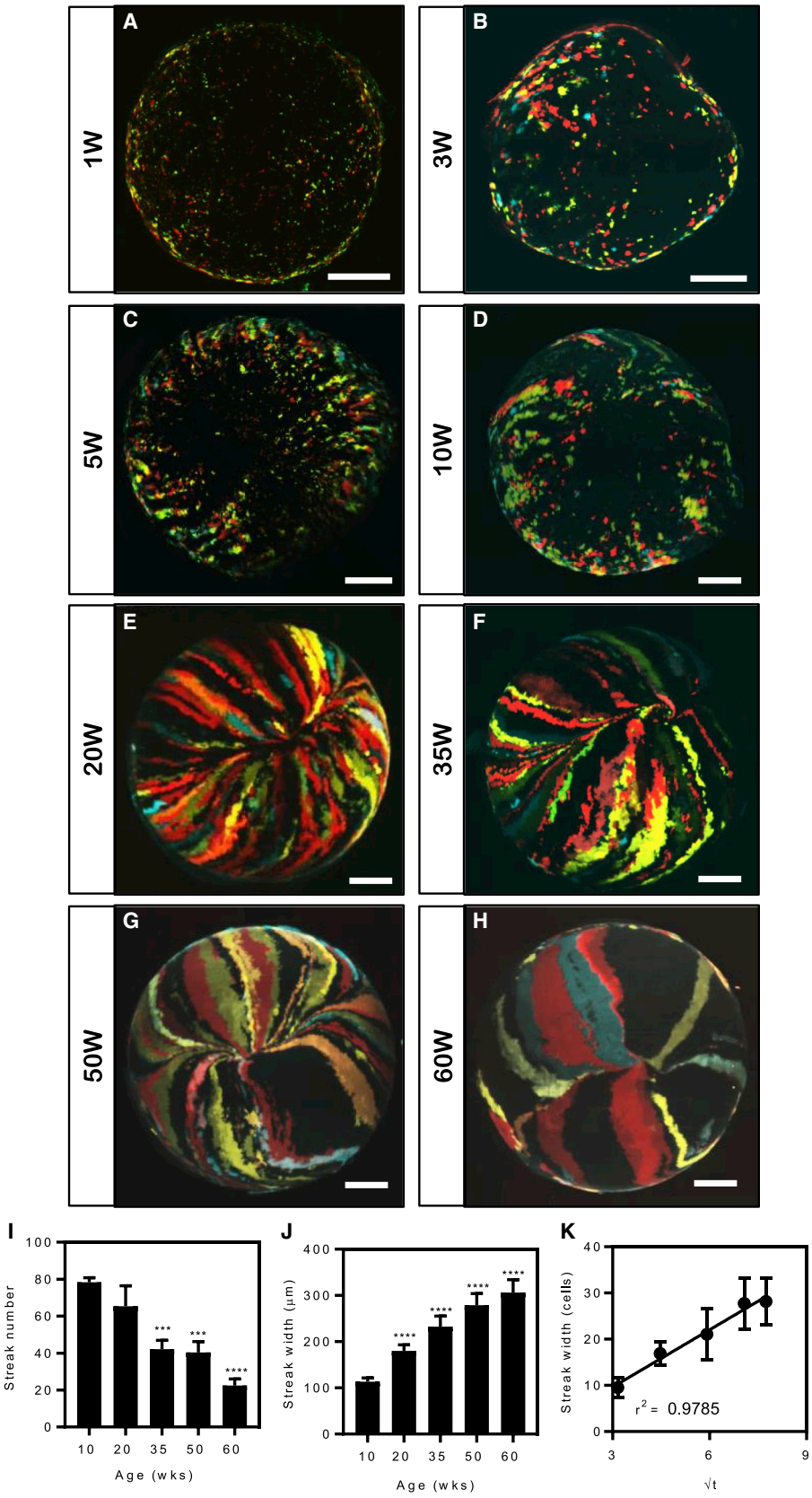

(legend on next page)

due to mechanical sheering forces from the eyelids, which increases desquamation. This could result in formation of a narrow zone of attrition, prompting epithelia to deviate from their normal migratory path (Rose and Lavin, 1987a). Although epithelial cells are continuously lost from the cornea under steady state, we propose this to be an additional and focal process. The detection of TUNEL$^+$ cells in whole mouse corneas (Figures 6B–6F) supports this proposition, whereby increased apoptosis was detected along the N-T mid-line compared with the S-I axis. Further evidence in support of this notion comes from our mathematical modeling (Figures 6G–6P), where control simulations displayed no clonal deviation and no mid-line formation over time (Movie S1). However, when the model was modified to include a normally distributed 0.1% cell loss along the N-T axis, a demarcation line became obvious over time (Movie S2).

The results presented here feature the use of a robust lineage-tracing tool, state-of-the-art imaging modalities, and advanced computational models to determine the fate of a rare population of SCs and their progeny in a transparent, external organ system that uniquely enables real-time intra-vital imaging. Our data demonstrate that K14$^+$ progenitor cells are designated early and widely distributed in the embryonic cornea. We are also first to report in a mammalian system, the biphasic nature of corneal epithelial development. During post-natal development, these cells become sequestered into the confines of the limbus where they actively support a narrow radial wedge of corneal epithelia (Figure 7). Our findings are significant on three levels. Firstly, they deliver an accurate visual fate-map of corneo-limbal SC and their life-long clonal activity. Secondly, we provide mechanistic explanations for age-related patterns within the epithelium over time, using both *in vivo* and *in silico* investigations. Lastly, these results provide the foundations of a model that can be used to interrogate perturbations of the cornea, including wound healing, infection, and transplantation. Such future studies will have profound implications for understanding the basic biology of the cornea and for devising novel strategies to treat corneal diseases.

EXPERIMENTAL PROCEDURES

K14CreER^{T2}-Confetti Mice

All animal procedures were performed in accordance with UNSW Animal Care and Ethics Committee guidelines (approval no. 14/89B) and the Australian Code of Practice for the Care and Use of Animals for Scientific Purposes. The transgenic mice used in this study have been described previously (Di Girolamo et al., 2015; Lobo et al., 2016). Genotyping was performed on tail tips from 2-week-old mice, and both males and females homozygous for the Confetti transgene were used. Timed mating was performed and the presence of a vaginal plug indicated E0.5, while birth was designated as P0. Transgene recombination was induced with tamoxifen (Sigma-Aldrich) dissolved in 10% ethanol and 90% olive oil (Sigma-Aldrich) at a concentration of 5 mg/mL. Pregnant transgenic mice were administered a single intraperitoneal (i.p.) TAM dose of 100 μg/g bodyweight at E15.5. Other mice were administered 50 μg/g bodyweight on three consecutive days when they were between 1 and 59 weeks of age.

Clonal Analysis in Embryos and Neonates

Pregnant transgenic mice were euthanized between E16.5 and E19.5 by cervical dislocation; embryos were surgically removed, fixed in 4% paraformaldehyde (PFA) (Sigma-Aldrich) overnight at 4°C, then stored in 0.5% PFA at 4°C until further use. Neonatal pups were harvested at P7 and P14. Embryos and P7 pups were separated based on genotype, the eyelid skin was surgically removed and corneas imaged on an SP5 2P STED (Leica Microsystems) fluorescent confocal microscope. Pups at P14 had their eyes enucleated, corneas dissected, and imaged on an LSM 780 (Carl Zeiss, Jena, Germany) confocal microscope. Images were analyzed with FiJi software (Schindelin et al., 2012). A clone was defined as a coherent cluster of >2 fluorescent cells of the same color combination, visibly separated from its neighbor.

Monitoring K14$^+$ Clonal Location and Dynamics during Aging

Confetti mice of varying ages (1–60-weeks-old) were administered TAM and either (1) monitored by intra-vital microscopy for 10 weeks to observe changes to the fluorescent pattern, (2) euthanized 1 week post TAM, their corneas flat-mounted and imaged by confocal microscopy, or (3) imaged by intra-vital microscopy 3 weeks post TAM, then every 4 weeks for a period of up to 60 weeks.

Figure 5. Evolving Multi-colored Corneal Clones during Aging

(A–H) Light-sheet microscopy of Confetti corneas (n = 3 corneas/time point) following a chase period of 1 (A), 3 (B), 5 (C), 10 (D), 20 (E), 35 (F), 50 (G), and 60 (H) weeks (W).

(I) Light-sheet images analyzed for streak number (n = 3 corneas/time point ±SD, ***p < 0.001 and ****p < 0.0001, one-way ANOVA with Holm-Sidak multiple comparisons test).

(J) Light-sheet images analyzed for streak width (n = 3 corneas/time point ±SD, ****p < 0.0001, one-way ANOVA with Holm-Sidak multiple comparisons test).

(K) The width of fluorescent streaks (in number of cells) against the inverse square root of the appropriate time point. The width of the streaks was transformed from micrometers to number of cells based on the average width of a corneal epithelial basal cell of 10 μm. Data points represent the mean (n = 3 corneas/time point, ± SD, linear regression).

Scale bars (A–H), 400 μm. See also Figure S3.

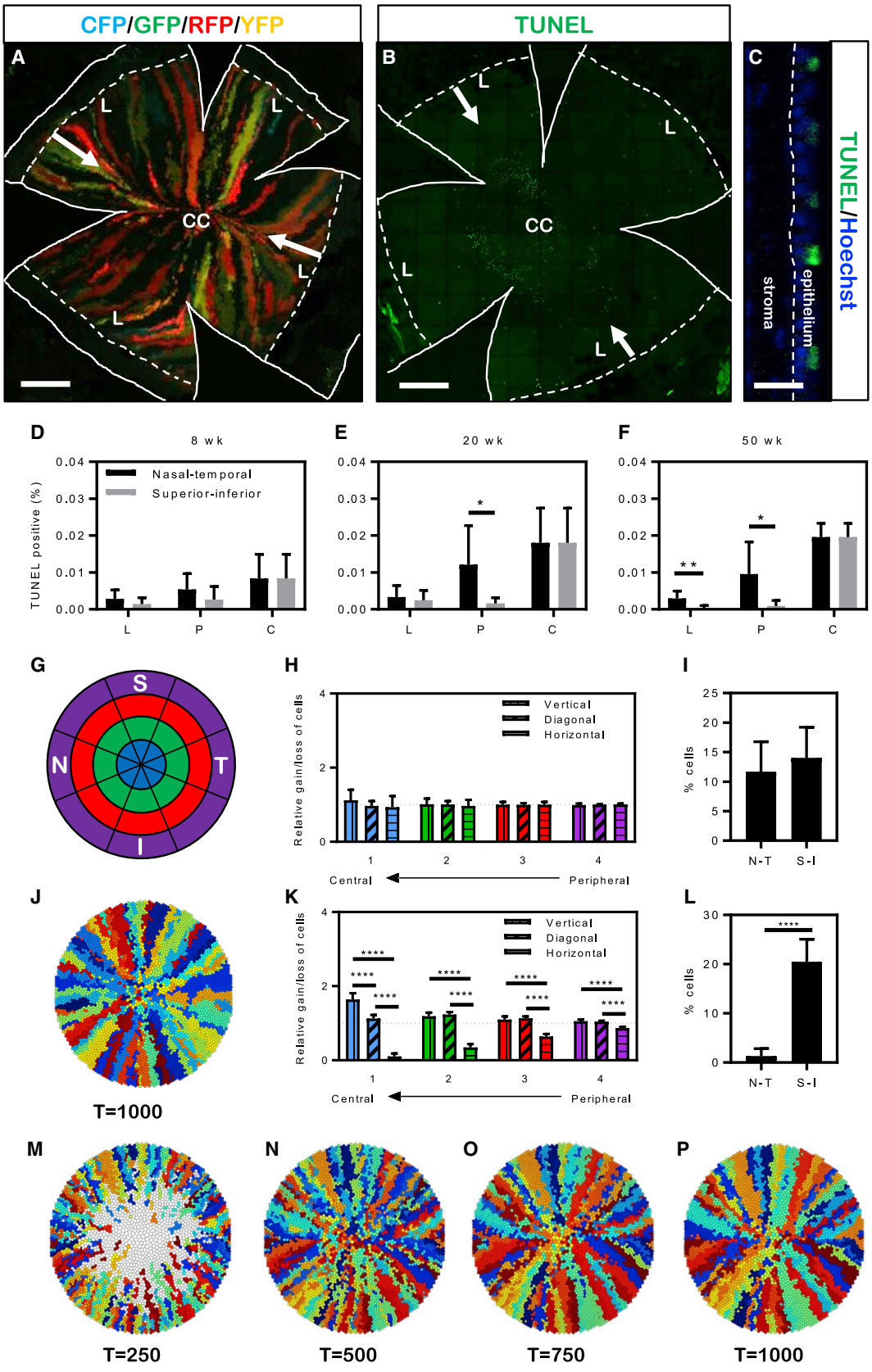

(legend on next page)

Mice euthanized 1 week post TAM administration had their eyes enucleated, fixed in 4% PFA overnight at 4°C, corneas dissected, washed in PBS, flat-mounted, scanned on an LSM 780 (Carl Zeiss) confocal microscope, and images imported into FiJi software. A series of equidistant concentric rings were digitally superimposed over each image, and fluorescence intensity within each region was measured and divided by the area of that region. Data were plotted on a histogram to ascertain the distribution of fluorescence (i.e., $K14^+$ cells) throughout the cornea (Lobo et al., 2016). Notably, this generates semi-quantitative data that do not provide an absolute cell count.

Intra-vital microscopy was performed on mice anesthetized with 100 μg/g ketamine (Provet) and 10 μg/g xylazine (Sigma-Aldrich). In brief, corneas were irrigated with sterile saline eye drops (Irripod, Merlin Medical) and mice placed under a 3i VIVO (Intelligent Imaging Innovations) fluorescent microscope in a custom-made restraint; images were acquired through four filters (CFP, GFP, YFP, and RFP) and processed using SlideBook v6 (Intelligent Imaging Innovations) and FiJi software (Schindelin et al., 2012).

Analysis of Clonal Dynamics during Aging

Cell migration rate was estimated by measuring three streaks of each color (YFP, RFP, and CFP) from when they emerged from the limbus until they reached the apex of the cornea. Data generated from each eye (per time point) were pooled and the average migration rate was calculated in μm/day.

The number of fluorescent streaks was established by counting them in one-third of the cornea and multiplying this value by 3. An exact count could not be obtained as one-third of the ocular surface was in sharp focus. Streak number was also calculated using images generated from light-sheet microscopy. Average streak width was estimated from both intra-vital and light-sheet microscopy images. Measurements were taken at the limbus, and data at each time point were pooled to generate the average width.

TUNEL Staining

Wild-type C57BL/6 mice at various ages were euthanized by cervical dislocation, and their eyes were marked at temporal and nasal positions by a 25G needle puncture. Eyes were enucleated, fixed in 4% PFA overnight at 4°C, then washed in TBS, and corneas dissected. TUNEL staining was performed using a DeadEnd Fluorometric TUNEL Assay kit (Promega) as previously described (Lobo et al., 2016), and samples were counterstained with Hoechst nuclear stain (Invitrogen).

Mathematical Model

We previously developed and validated a mathematical model in MATLAB (MathWorks) based on free-lattice, discrete-state geometric structures known as Voronoi diagrams, which contains

Figure 6. $TUNEL^+$ Cell Distribution during Aging and *In Silico* Analysis of Increased Central Corneal Cell Loss over Time

(A) Flat-mounted cornea 20 weeks post TAM. White arrows represent the N-T demarcation, solid white lines indicate incisions made to facilitate flattening, and hatched white lines depict the limbal border.

(B) Flat-mounted cornea highlighting $TUNEL^+$ cells (green). White arrows represent the N-T axis. Solid white lines indicate incisions made to facilitate flattening and hatched white lines depict the limbal border.

(C) Orthogonal view of $TUNEL^+$ cells (green) within the corneal epithelium. Samples were counterstained with Hoechst 33342 nuclear stain (blue). The white hatched line represents the epithelial basement membrane.

(D–F) Percentage TUNEL-positive cells at 8 (D), 20 (E) and 50 (F) weeks of age was calculated from limbal, peripheral, and central corneal regions and plotted on histograms. Bars represent the mean (n = 4–5 corneas/time point ±SD, *p < 0.05, **p < 0.01, Welch's t test with unequal variance). L, limbal; P, peripheral; C, central.

(G) Representative sectors and zones that were used to divide simulations on corneas. The regions were composed of the following sectors: vertical was superior (S) combined with inferior (I), horizontal was nasal (N) combined with temporal (T), and diagonal was the remaining four sectors. Colors are representative of concentric zone 1 (blue), 2 (green), 3 (red), 4 (purple) in (H) and (K).

(H) Simulations performed in control corneas without increased cell loss, comparing relative cell loss/gain across the pooled vertical, horizontal, and diagonal axes. The relative loss/gain was calculated by dividing the observed proportion of cells in each zone sector that is derived from a LESC in the same sector by the predicted proportion if clonal growth was ideally centripetal (0.25, 0.50, and 0.25 for vertical, diagonal, and horizontal regions, respectively). Bars represent the mean (n = 20 simulations, ±SD, multiple t test with Holm-Sidak multiple comparisons).

(I) The average percentage of cells within the central zone of simulations performed on control corneas that arose from progenitors within the periphery of the same sector in either the N-T or S-I axis. Bars represent the mean (n = 20 simulations, ± SD, Welch's t test).

(J) Simulated control cornea following 1,000 time steps.

(K) Simulations conducted in corneas that included a 0.1% rate of cell loss, normally distributed across the N-T axis, comparing net cell loss/gain across the pooled vertical, horizontal, and diagonal axes. Bars represent the mean (n = 20 simulations, ±SD, ****p < 0.0001, multiple t test with Holm-Sidak multiple comparisons).

(L) The average percentage of cells within the central zone that arose from a progenitor cell within the periphery of either wedge of the N-T or S-I axis of a simulated cornea that includes a 0.1% rate of cell loss. Bars represent the mean (n = 20 simulations, ±SD, ****p < 0.0001, Welch's t test with unequal variance).

(M–P) Simulations conducted in corneas that included a 0.1% increased rate of cell loss as time proceeds from t = 250 (M), t = 500 (N), t = 750 (O) to t = 1,000 (P).

Scale bars: (A and B) 500 μm, (C) 50 μm. See also Figure S4, Movies S1 and S2.

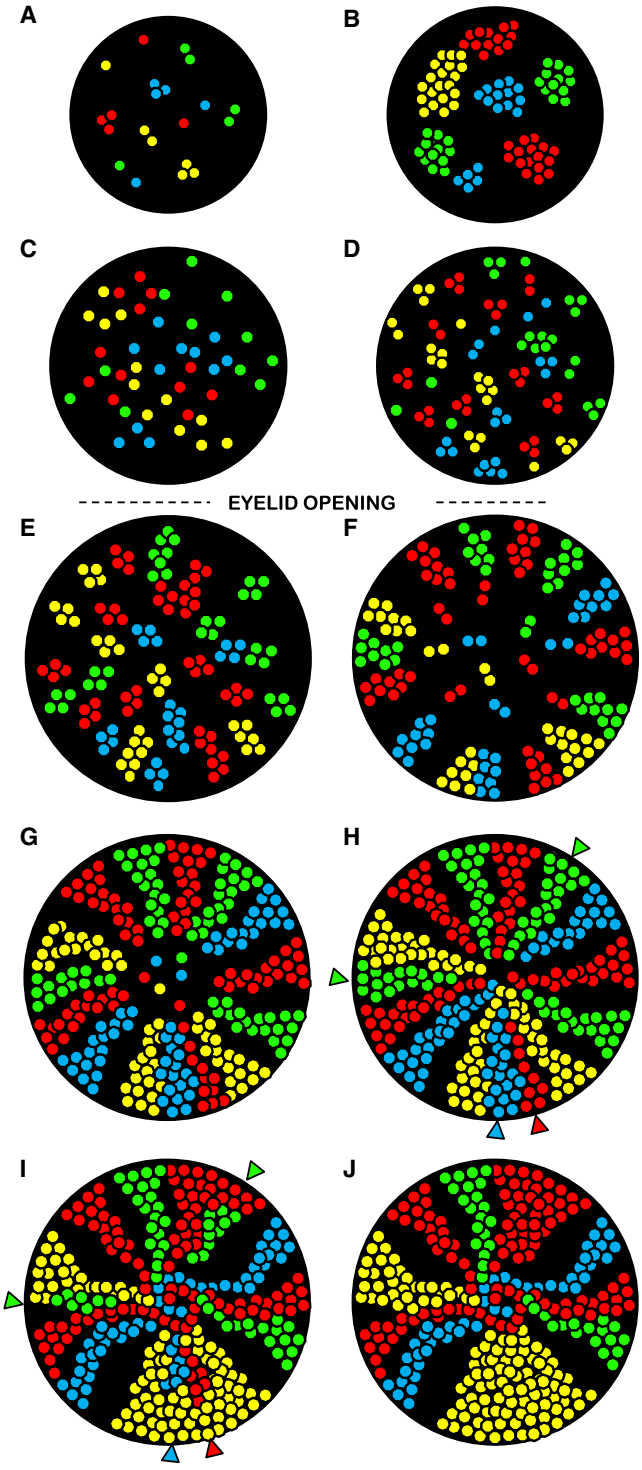

Figure 7. A Model to Describe Clonal Dynamics in the Mouse Cornea

The schema depicts developmental stages of the corneal epithelium from Confetti mice. Black circles (not to scale) represent corneas at; E16.5 (A), E18.5 (B), E19.5 (C), P7 (D), P14 (E), 4 (F), 10 (G), 20 (H), 40 (I), and 60 (J) weeks. Notably, K14 is initially expressed on the corneal surface at approximately E14.5 to E15 (Kurpakus et al., 1994; Tanifuji-Terai et al., 2006); in our model, they are the precursor cells that spawn small cohesive clones of <5 cells at E16.5 (A) which expand in size until E18.5 (B). Between E18.5 and E19.5 (C) cells within each clone begin to scatter across the corneal surface. In turn, individual cells seed new colonies that continue to expand until P7 (D), after which they begin aligning radially by P14; this activity coincides with eyelid opening (E). Once eyelids open, corneal epithelial cells are subject to environmental stressors (i.e., UV radiation and microbes) and intrinsic friction forces from blinking, leading to the gradual decline of centrally located clones, and by 4 weeks of age, the emergence of limbal-predominating counterparts (F). By 10 weeks, central clones all but disappear, rendering limbal colonies responsible for maintaining corneal epithelial mass (G), which persists until approximately 20 weeks of age (H). However, this arrangement is not static as SCs are known to be lost during aging (Klein and Simons, 2011). A decline in SC number might render arcs of limbal tissue devoid of progenitors, forcing neighboring SCs to divide symmetrically and take on the role of tissue maintenance. In our model, this is visualized as the loss of a fluorescent clone and the broadening of neighboring colony (colored arrowheads in H and I). When fluorescent streaks meet at the cornea's apex, a vortex can form due to converging forces (I and J). Finally, fluorescent clones can deviate from their typical linear path and bend toward the central cornea.

4,000 cells, approximately one-third the diameter of a mouse cornea (Lobo et al., 2016). Based on our *in vivo* results, we modified our simulations to introduce one additional component; namely, the removal of cells close to the N-T mid-line of the cornea.

The additional probability p* that any cell within the cornea is removed at a single time step is given by

$$p* = \frac{1}{\kappa_1}\varphi\left(\frac{c_y}{\kappa_2}\right),$$

where c_y is the perpendicular distance from the cell to the nasal temporal mid-line measured in units of corneal radii, $\varphi(x)$ is the standard normal distribution; $\kappa_1 = 0.8$ and $\kappa_2 = 275$ are parameters chosen so that there is an additional removal of approximately 0.1% of cells around the horizontal axis of the cornea per time step.

The parameter that represents the rate of proliferation of SCs was also adjusted to maintain equilibrium within the cell population of the simulated cornea.

Quantification and Statistical Analysis

All statistical methods are described in the figure legends; a p value of <0.05 was considered significant. Unless otherwise stated, all data are displayed as means ± SD with asterisks denoting significance between groups. Unless stated otherwise, all data were analyzed by one-way ANOVA with a Hölm-Sidak multiple comparisons test.

SUPPLEMENTAL INFORMATION

Supplemental Information includes Supplemental Experimental Procedures, four figures, and two movies and can be found with

this article online at http://dx.doi.org/10.1016/j.stemcr.2017.08.015.

AUTHOR CONTRIBUTIONS

Conceptualization, A.R., N.D., J.G.L., D.W., and M.R.M.; Methodologies, A.R., E.P.L., N.C.D., and J.G.L.; Investigation, A.R., E.P.L., and N.C.D.; Resources, N.D., D.W., J.G.L., and M.R.M.; Writing – Original Draft, A.R. and N.D.; Writing – Review and Editing, A.R., E.P.L., N.C.D., M.R.M., J.G.L., D.W. and N.D.; Supervision, N.D., D.W., and J.G.L.; Funding Acquisition, N.D. and J.G.L.

ACKNOWLEDGMENTS

The authors would like to thank Richard Francis, Sandra Fok, and Iveta Slapetova (Biomedical Imaging Facility, University of New South Wales, Sydney, Australia) for their assistance with intra-vital, confocal, and light-sheet microscopy and image analysis and Daniel Metzger and Pierre Chambon (Institut Génétique Biologie Moléculaire Cellulaire, Cedex, France) for providing the K14CreER^{T2} mouse strain. Funding: The Australian National Health and Medical Research Council (APP1101078) and Human Frontiers Research Program, Worldwide Cancer Research.

Received: April 4, 2017
Revised: August 23, 2017
Accepted: August 23, 2017
Published: September 21, 2017

REFERENCES

Auran, J.D., Koester, C.J., Kleiman, N.J., Rapaport, R., Bomann, J.S., Wirotsko, B.M., Florakis, G.J., and Koniarek, J.P. (1995). Scanning slit confocal microscopic observation of cell morphology and movement within the normal human anterior cornea. Ophthalmology *102*, 33–41.

Beebe, D.C., and Masters, B.R. (1996). Cell lineage and the differentiation of corneal epithelial cells. Invest. Ophthalmol. Vis. Sci. *37*, 1815–1825.

Bron, A.J. (1973). Vortex patterns of the corneal epithelium. Trans. Ophthalmol. Soc. UK *93*, 455–472.

Buck, R.C. (1985). Measurement of centripetal migration of normal corneal epithelial cells in the mouse. Invest. Ophthalmol. Vis. Sci. *26*, 1296–1299.

Collinson, J.M., Morris, L., Reid, A.I., Ramaesh, T., Keighren, M.A., Flockhart, J.H., Hill, R.E., Tan, S.S., Ramaesh, K., Dhillon, B., et al. (2002). Clonal analysis of patterns of growth, stem cell activity, and cell movement during the development and maintenance of the murine corneal epithelium. Dev. Dyn. *224*, 432–440.

Davanger, M., and Evensen, A. (1971). Role of the pericorneal papillary structure in renewal of corneal epithelium. Nature *229*, 560–561.

Di Girolamo, N., Bobba, S., Raviraj, V., Delic, N.C., Slapetova, I., Nicovich, P.R., Halliday, G.M., Wakefield, D., Whan, R., and Lyons, G.J. (2015). Tracing the fate of limbal epithelial progenitor cells in the murine cornea. Stem Cells *33*, 157–169.

Dora, N.J., Hill, R.E., Collinson, J.M., and West, J.D. (2015). Lineage tracing in the adult mouse corneal epithelium supports the limbal epithelial stem cell hypothesis with intermittent periods of stem cell quiescence. Stem Cell Res. *15*, 665–677.

Doupe, D.P., Alcolea, M.P., Roshan, A., Zhang, G., Klein, A.M., Simons, B.D., and Jones, P.H. (2012). A single progenitor population switches behavior to maintain and repair esophageal epithelium. Science *337*, 1091–1093.

Dua, H.S., and Gomes, J.A. (2000). Clinical course of hurricane keratopathy. Br. J. Ophthalmol. *84*, 285–288.

Eghtedari, Y., Richardson, A., Mai, K., Heng, B., Guillemin, G.J., Wakefield, D., and Di Girolamo, N. (2016). Keratin 14 expression in epithelial progenitor cells of the developing human cornea. Stem Cells Dev. *25*, 699–711.

Every, S.G., Leader, J.P., Molteno, A.C., Bevin, T.H., and Sanderson, G. (2005). Ultraviolet photography of the in vivo human cornea unmasks the Hudson-Stahli line and physiologic vortex patterns. Invest. Ophthalmol. Vis. Sci. *46*, 3616–3622.

Gass, J.D. (1964). The iron lines of the superficial cornea. Arch. Ophthalmol. *71*, 348–358.

Hsueh, Y.J., Wang, D.Y., Cheng, C.C., and Chen, J.K. (2004). Age-related expressions of p63 and other keratinocyte stem cell markers in rat cornea. J. Biomed. Sci. *11*, 641–651.

Iannaccone, S., Zhou, Y., Walterhouse, D., Taborn, G., Landini, G., and Iannaccone, P. (2012). Three dimensional visualization and fractal analysis of mosaic patches in rat chimeras: cell assortment in liver, adrenal cortex and cornea. PLoS One *7*, e31609.

Indra, A.K., Dupe, V., Bornert, J.M., Messaddeq, N., Yaniv, M., Mark, M., Chambon, P., and Metzger, D. (2005). Temporally controlled targeted somatic mutagenesis in embryonic surface ectoderm and fetal epidermal keratinocytes unveils two distinct developmental functions of BRG1 in limb morphogenesis and skin barrier formation. Development *132*, 4533–4544.

Klein, A.M., and Simons, B.D. (2011). Universal patterns of stem cell fate in cycling adult tissues. Development *138*, 3103–3111.

Kurpakus, M.A., Maniaci, M.T., and Esco, M. (1994). Expression of keratins K12, K4 and K14 during development of ocular surface epithelium. Curr. Eye Res. *13*, 805–814.

Li, J., Xiao, Y., Coursey, T.G., Chen, X., Deng, R., Lu, F., Pflugfelder, S.C., and Li, D.Q. (2017). Identification for differential localization of putative corneal epithelial stem cells in mouse and human. Sci. Rep. *7*, 5169.

Lobo, E.P., Delic, N.C., Richardson, A., Raviraj, V., Halliday, G.M., Di Girolamo, N., Myerscough, M.R., and Lyons, J.G. (2016). Self-organized centripetal movement of corneal epithelium in the absence of external cues. Nat. Commun. *7*, 12388.

Lwigale, P.Y. (2015). Corneal development: different cells from a common progenitor. Prog. Mol. Biol. Transl. Sci. *134*, 43–59.

Majo, F., Rochat, A., Nicolas, M., Jaoude, G.A., and Barrandon, Y. (2008). Oligopotent stem cells are distributed throughout the mammalian ocular surface. Nature *456*, 250–254.

Mann, I. (1944). A study of epithelial regeneration in the living eye. Br. J. Ophthalmol. *28*, 26–40.

Mort, R.L., Ramaesh, T., Kleinjan, D.A., Morley, S.D., and West, J.D. (2009). Mosaic analysis of stem cell function and wound healing in the mouse corneal epithelium. BMC Dev. Biol. *9*, 4.

Nagasaki, T., and Zhao, J. (2003). Centripetal movement of corneal epithelial cells in the normal adult mouse. Invest. Ophthalmol. Vis. Sci. *44*, 558–566.

Pan, Y.A., Freundlich, T., Weissman, T.A., Schoppik, D., Wang, X.C., Zimmerman, S., Ciruna, B., Sanes, J.R., Lichtman, J.W., and Schier, A.F. (2013). Zebrabow: multispectral cell labeling for cell tracing and lineage analysis in zebrafish. Development *140*, 2835–2846.

Patel, D.V., and McGhee, C.N. (2005). Mapping of the normal human corneal sub-basal nerve plexus by in vivo laser scanning confocal microscopy. Invest. Ophthalmol. Vis. Sci. *46*, 4485–4488.

Ren, H., and Wilson, G. (1996). The cell shedding rate of the corneal epithelium–a comparison of collection methods. Curr. Eye Res. *15*, 1054–1059.

Rose, G.E., and Lavin, M.J. (1987a). The Hudson-Stahli line. II: a comparison of properties in eyes with and without long-term contact lens wear. Eye (Lond.) *1* (Pt 4), 471–474.

Rose, G.E., and Lavin, M.J. (1987b). The Hudson-Stahli line. III: observations on morphology, a critical review of aetiology and a unified theory for the formation of iron lines of the corneal epithelium. Eye (Lond.) *1* (Pt 4), 475–479.

Schindelin, J., Arganda-Carreras, I., Frise, E., Kaynig, V., Longair, M., Pietzsch, T., Preibisch, S., Rueden, C., Saalfeld, S., Schmid, B., et al. (2012). Fiji: an open-source platform for biological-image analysis. Nat. Methods *9*, 676–682.

Snippert, H.J., van der Flier, L.G., Sato, T., van Es, J.H., van den Born, M., Kroon-Veenboer, C., Barker, N., Klein, A.M., van Rheenen, J., Simons, B.D., et al. (2010). Intestinal crypt homeostasis results from neutral competition between symmetrically dividing Lgr5 stem cells. Cell *143*, 134–144.

Stepp, M.A., Tadvalkar, G., Hakh, R., and Pal-Ghosh, S. (2016). Corneal epithelial cells function as surrogate Schwann cells for their sensory nerves. Glia http://dx.doi.org/10.1002/glia.23102.

Tanifuji-Terai, N., Terai, K., Hayashi, Y., Chikama, T., and Kao, W.W. (2006). Expression of keratin 12 and maturation of corneal epithelium during development and postnatal growth. Invest. Ophthalmol. Vis. Sci. *47*, 545–551.

Thoft, R.A., and Friend, J. (1983). The X, Y, Z hypothesis of corneal epithelial maintenance. Invest. Ophthalmol. Vis. Sci. *24*, 1442–1443.

Yamamoto, K., Ladage, P.M., Ren, D.H., Li, L., Petroll, W.M., Jester, J.V., and Cavanagh, H.D. (2002). Effect of eyelid closure and overnight contact lens wear on viability of surface epithelial cells in rabbit cornea. Cornea *21*, 85–90.

Zieske, J.D. (2004). Corneal development associated with eyelid opening. Int. J. Dev. Biol. *48*, 903–911.